Vibroseis Monitoring of San Andreas Fault in California

Valeri Korneev and Robert Nadeau

Lawrence Berkeley National Laboratory, Berkeley, California, USA (VK)
University of California at Berkeley, Berkeley, California, USA (RN)

ABSTRACT

A unique data set of seismograms for 720 source-receiver paths has been collected as part of a controlled source Vibroseis experiment San Andreas Fault (SAF) at Parkfield. In the experiment, seismic waves repeatedly illuminated the epicentral region of the expected M6 event at Parkfield from June 1987 until November 1996. For this effort, a large shear-wave vibrator was interfaced with the 3-component (3-C) borehole High-Resolution Seismic Network (HRSN), providing precisely timed collection of data for detailed studies of changes in wave propagation associated with stress and strain accumulation in the fault zone (FZ). Data collected by the borehole network were examined for evidence of changes associated with the nucleation process of the anticipated M6 earthquake at Parkfield These investigations reported significant traveltime changes in the S coda for paths crossing the fault zone southeast of the epicenter and above the rupture zone of the 1966 M6 earthquake. Analysis and modeling of these data and comparison with observed changes in creep, water level, microseismicity, slip-at-depth and propagation from characteristic repeating microearthquakes showed temporal variations in a variety of wave propagation attributes that were synchronous with changes in deformation and local seismicity patterns. Numerical modeling suggests 200 meters as an effective thickness of SAF. The observed variations can be explained by velocity 6% velocity variation within SAF core.

Numerical modeling studies and a growing number of observations have argued for the propagation of fault-zone guided waves (FZGW) within a SAF zone that is 100 to 200 m wide at seismogenic depths and with 20 to 40% lower shear-wave velocity than the adjacent unfaulted rock. Guided wave amplitude tomographic inversion for SAF using microearthquakes, shows clearly that FZGW are significantly less attenuated in a well-defined region of the FZ. This region plunges to the northwest along the northwest boundary of the region of highest moment release and separates locked and slipping sections of the SAF at depth, as determined independently from geodesy, seismicity and the recurrence rates of characteristically repeating microearthquakes. The mechanism for low FZGW attenuation in the zone is possibly due to dewatering by fracture closure and/or fault-normal compression, or changes in fracture orientation due to a complex stress or strain field at the boundary between creeping and locked zones of the San Andreas Fault. Temporal changes of FZGW correlates with changes in overall seismicity. Active monitoring of changes in FZGW has a potential for imaging and detecting of changes in strees within FZ cores. Since FZGW primarily propagate in the low-velocity core region of fault zones, they sample the most active zone of fault deformation and provide greater structural detail of the inner fault core than body waves which propagate primarily outside of the central core region. FZGW also can be used for FZ continuity studies.

KEYWORDS: active monitoring, Vibroseis, guided waves, Parkfield

INTRODUCTION

The town of Parkfield, located on the San Andreas Fault in central California, has been the site of intensive, multidisciplinary earthquake studies since the 1970s. Moderate-sized earthquakes of about magnitude 6 have occurred on the Parkfield section of the San Andreas Fault at fairly regular intervals—in 1857, 1881, 1901, 1922, 1934, and 1966. The 1857 event was a foreshock of the great Fort Tejon earthquake (magnitude 8¼), which ruptured the fault from Parkfield to the southeast for over 180 miles. Available data suggest that all six moderate-sized Parkfield earthquakes may have been "characteristic" in the sense that they all ruptured the same area on the fault. If such characteristic ruptures occur regularly, then the next quake is imminent. Current estimates of the likelihood of the next Parkfield earthquake are about 10% per year, and the possibility of it occurring as a foreshock to another Fort Tejon type event remains high. The goal of research in the Parkfield area has been to observe the fault and surrounding crust at close range and at high resolution before, during, and after a large damaging earthquake, so as to better understand the earthquake process and to provide a scientific basis for earthquake prediction and hazard assessment. Recognizing this hazard, and the regular periodicity of recurring events near Parkfield, the U.S. Geological Survey and the State of California began a comprehensive, long-term Parkfield Earthquake Prediction Project in [1]. More that 100 researchers have been involved various facets of this project.

HRSN

The HRSN (Figure 1), established at Parkfield, CA in 1987, records exceptionally high-quality data, owing to its 13 closely spaced three-component borehole sensors, its very broadband recordings (0-125 Hz), and its sensitivity (recording events below magnitude -0.5) [2]

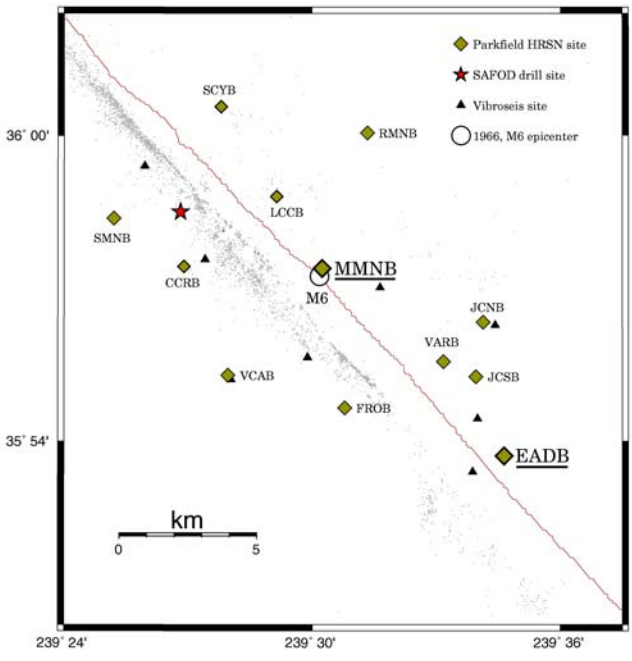

Figure 1. Map showing the San Andreas Fault trace, the location of the original 10 Parkfield HRSN stations. Relocated seismicity (1987 to 1998.5) is also shown (gray points) as are the locations of the 8 source points of the Vibroseis wave propagation monitoring experiment. The epicenter of the 1966 M6 Parkfield mainshock and location of the proposed San Andreas Fault Observatory at Depth (SAFOD) drill site are also shown [3].

Several aspects of the Parkfield region make it ideal for the study of seismic wave propagation and small earthquakes and their relation to tectonic processes. These include the fact that the network spans the expected nucleation region of a repeating magnitude 6 event and the transition from locked to creeping behavior on the San Andreas fault, the availability of three-dimensional P and S velocity models, a very complete seismicity catalogue, a well-defined and simple fault segment, and a homogeneous mode of seismic energy release as indicated by the earthquake source mechanisms. More than 6,000 earthquakes have been recorded since 1987 in the magnitude range -1<M<5. A recent expansion and upgrade improves the HRSN's capacity to image structure and slip kinematics at the SAFOD fault penetration site.

SAFOD project

SAFOD is a 4-km-deep observatory to be drilled directly into the San Andreas fault zone near the location of the 1966 magnitude 6 Parkfield earthquake. By revealing the physical and chemical processes acting deep within a seismically active fault, SAFOD will provide direct information on the composition and mechanical properties of fault rocks, the nature of stresses responsible for earthquakes, the role of fluids in controlling faulting and earthquake recurrence, and the physics of earthquake initiation and rupture. By drilling down to the earthquakes and observing them "close-up", SAFOD will represent a major opportunity to advance the pursuit of a rigorous scientific basis for earthquake hazard assessment and prediction. SAFOD 2 km deep pilot hole was completed in2002. The main drilling will begin west of the San Andreas Fault, and will use advanced directional-drilling technologies developed by the petroleum industry to drill an inclined hole through the entire fault zone until relatively undisturbed rock is reached on the other side. Fault-zone rocks and fluids will be retrieved for laboratory analyses, and intensive downhole geophysical measurement will be made within the active fault zone. The observatory's long-term monitoring activities will include decades of detailed seismological observations of small- to moderate-sized earthquakes, and continuous measurements of rock deformation and other parameters during the earthquake cycle. To provide a more detailed characterization of the region around the site of the deep drill hole and its 4 km deep target on the SAF, a 2 km deep "pilot" hole was drilled and instrumented with seismometers in 2002 near the surface location planned for the drilling rig, ~1.6 km SW of the San Andreas fault near Parkfield, CA. These seismometers are currently in place and operating, presenting a major opportunity for the controlled source experiment.

VIBROSEIS MONITORING

A unique data set of seismograms for 720 source-receiver paths has also been collected as part of a controlled source Vibroseis experiment. In the experiment, seismic waves repeatedly illuminated the epicentral region of the expected M6 event at Parkfield from June 1987 until November 1996. For this effort, a large shear-wave vibrator was interfaced with the 3-component (3-C) borehole HRSN, providing precisely timed collection of data for detailed studies of changes in wave propagation associated with stress and strain accumulation in the fault zone. Data collected by the borehole network were examined for evidence of changes associated with the nucleation process of the anticipated M6 earthquake at Parkfield [2,4]. These investigations reported significant traveltime changes in the S coda for paths crossing the fault zone southeast of the epicenter and above the rupture zone of the 1966 M6 earthquake. Progressively decreasing travel times through the anomalous region reached over 50 msec change by the end of the study. Changes in frequency content and polarization were also found that were localized to the zone of common nucleation and rupture onset for the previous M6 earthquakes and, possibly, the region of slip initiation for the great earthquake of 1857. Analysis and modeling of these data and comparison with observed changes in creep, water level, microseismicity, slip-at-depth and propagation from characteristic repeating microearthquakes showed temporal variations in a variety of wave propagation attributes that were synchronous with changes in deformation and local seismicity patterns [2,5,6,7,8].

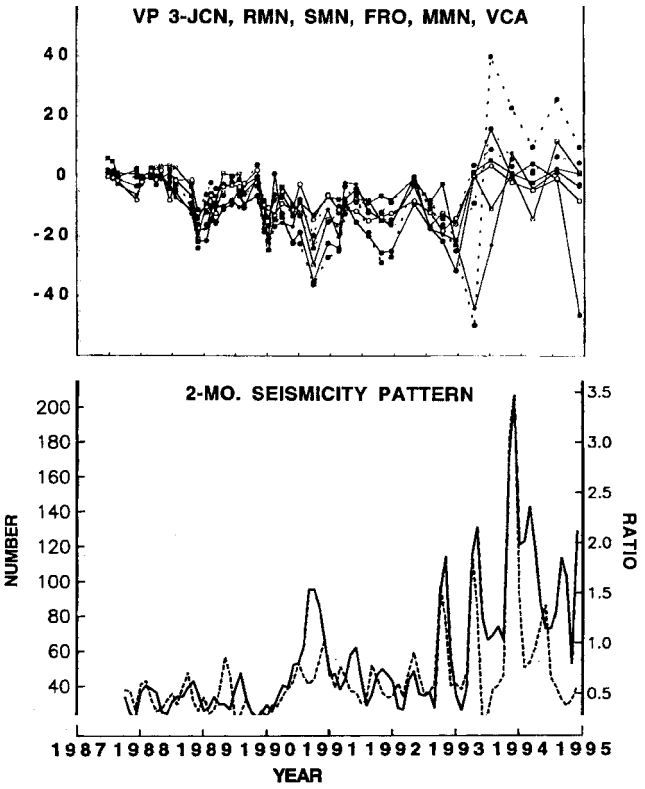

Figure 2. Comparative history of seismicity and traveltime changes for Vibroseis monitoring experiment (1987-1995).Top frame: Cumulative number of microearthquakes calculated for 2-month moving windows. Solid line shows total seismicity; dashed line shows the ratio of deep to shallow events(below and above 5 km in depth).The spikes are associated with the events of October 1992;March, April, and November of 1993; and December 1994. These sequences abruptly changed the dominant microearthquake activity from shallow to deep (ratio >1.0) Bottom frame: History of traveltime variations for 100 to 200-msec windows shows contrasting correlation with seismicity [4].

These studies also isolated the region of wave-propagation changes to the upper 3-4 km of the San Andreas Fault Zone, just above the locked zone of the expected M6 event. It was hypothesized that these localized changes were in response to changing fluid conditions in the upper crust induced by tectonic deformation and stress and strain accumulation in the locked section of the fault at depth. Additionally, vibroseis VSP experiments in the nearby Varian well measured and monitored shear-wave anisotropy at [9,10].

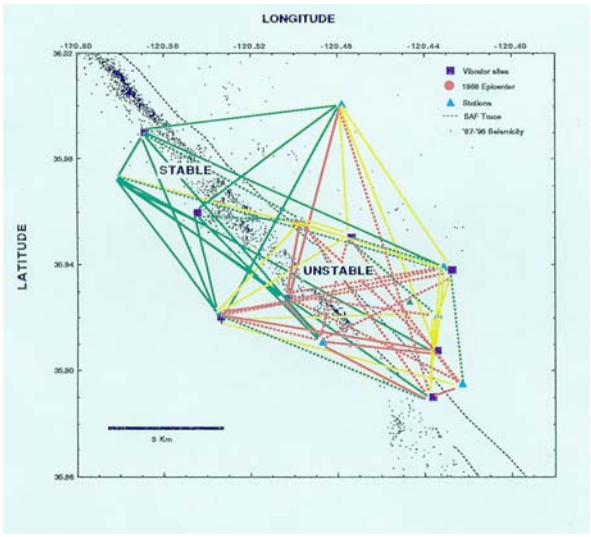

Figure 3.. All source-receiver paths for the full data set showing special distribution of the observed time advances for S- coda; solid red lines represent the greatest change; solid grin lines, the most stable travel times. Yellow lines represent paths showing small variation. The changes are concentrated in the region labeled unstable southeast of Middle Mountain, associated with locked zone of the SAF [4].

Origin of Changes

At Parkfield the San Andreas fault zone is a striking near-vertical low-velocity zone , and it very clearly acts as a waveguide for seismic energy from earthquakes on the fault and from surface sources . Velocity models there show high Vp/Vs ratio along the fault near the surface and at depth within the fault zone, and a pronounced vertical velocity gradient in the upper 2 km of the section. The geometry of the Vibroseis source and receiver network, the approximate two-dimensionality of the fault zone in the region of the travel-time anomaly, and the existence of detailed P- and S-wave velocity models for the area all combine to provide well-determined constraints in modeling the observations. In [] study only data recorded at stations VCA and JCN from vibrator site VP2 were considered. At VP2 we have the routine Vibroseis monitoring data from the repeated point source, as well as a cross array of sources with 17 VPs on each leg. We confined our modeling exercise to the VP2 data for VCA and JCN for several reasons. Both source-receiver paths are in the anomalous region and reveal substantial travel-time variations. The two paths are approximately co-linear and orthogonal to the San Andreas fault, permitting the use of a two-dimensional formulation in simulating wave propagation. The paths sample segments of similar-length on the two sides of the fault zone. Finally, the data profile from the closely-spaced source array at VP2 defines the spatial coherency of the wavefield that is helpful in phase identification and interpretation of the recorded wavefield. The velocity model used in numerical simulation incorporates the known properties of the region, where tomographic three-dimensional velocity models have already been determined . A major factor controlling the character of wave propagation at short range from a surface source is the severity of the shallow vertical velocity gradient. We found a velocity gradient model by matching the observed and computed direct arrivals in the early part of seismograms. For the NE side of the fault, the direct arrivals at JCN could be matched with a velocity profile reduced to 0.76 of that for VCA, and to 0.5 for the narrow fault zone, modeled as a vertical layer with a thickness of 200 meters, bounded by interfaces F1 and F2 . Computations were performed using a two-dimensional elastic finite-difference formulation with a staggered grid. The model was digitized on a 2200 x 500 grid with 5m spacing, which yields a model space of 11 km horizontal and 2.5 km vertical extent, as depicted in the figure.

A snapshot of elastic field development is presented in Figure 4. Two features dominate the process: energy trapping near the surface by the shallow gradient, and wavefield scattering from the fault zone. Most of the energy is confined to the upper part of the section in multiple reflections at the free surface, producing a complex train of surface-guided waves made up of many arriving phases.

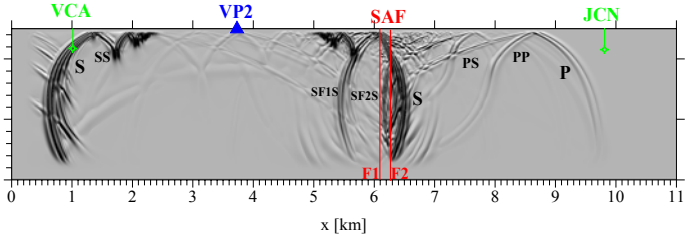

Figure 4. Computed wavefield snapshot at 2 seconds. The narrow low-velocity fault zone (SAF) is bounded by vertical interfaces F1 and F2. The panel shows the P and S waves passing VCA and the SAF at 1 and 2 seconds, respectively. Within the coda, distinct reflected S waves SF_1S and SF_2S from the F1 and F2 boundaries are approaching VCA.

Initial direct P and S waves arrive around 1 sec and 2 sec at VCA. At JCN they are seen at 2.2 sec and 4.4 sec. Because the receivers are located at depth, both up- and down-going energy is seen, as well as horizontally propagating turning-point waves.

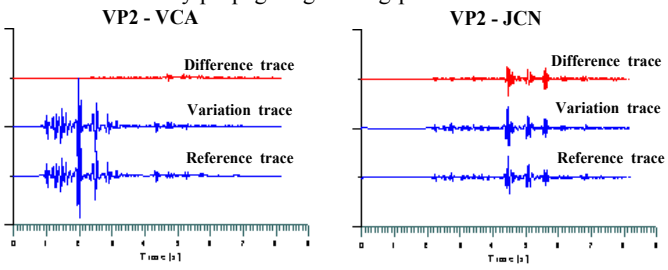

Figure 5. Synthetic traces for variation modeling [8].

The signature of the fault zone and shallow gradient on the wavefield is dramatic. In the interval between the first-arriving P and S waves at VCA are the surface-generated multiples and conversions. The latter are especially strong for P-waves, e.g., PS, PPS, etc. Strong reflections are also produced by the fault-zone boundaries, F1 and F2 . PF_1P, the first F1 reflection at VCA, is small and masked by the large direct S wave just before it. F2 reflections at VCA have passed twice through the fault zone, and these late phases such as PF_2PP (3.5s) and SF_2S (4.7s) are quite strong, arriving well after the direct waves have passed . At JCN the internal fault-zone reflections produce sequences of strong, distinct arrivals following the direct P and S waves. The times in the synthetic seismograms where large travel-time changes were observed in the monitoring project at VCA and JCN contain significant energy that has been scattered from the fault zone. This result suggests a ready explanation for the cause of the observed progressively decreasing travel-times . For the path VP2-VCA the changes were seen at arrival times after 3.5 seconds, i.e., for our model seismograms, after the direct waves have passed and the fault-zone reflected waves are arriving. On the other hand, the travel-time changes for the VP2-JCN fault-crossing path begin with the arrival of the direct P wave and occur through the entire seismogram. We take these results to be strong evidence that the observed variations are most likely caused by changes within the fault zone itself. To test the fault-zone hypothesis we modeled travel-time variations that would be produced by a small velocity change at the fault. To compare with seismograms for the reference model described above, we computed new seismograms at VCA and

JCN for a velocity increase of 6% localized in the narrow fault zone. These seismograms are shown in Figure 5 along with their differences from the reference traces. As expected, the changes at VCA appear only after the fault-zone F2 reflections reach the station, while at JCN the travel-time advance begins with the initial P wave and increases throughout the seismogram. The magnitude of the calculated travel-time variations match the observed data quite closely. In Figure 6 we make a direct comparison with the Vibroseis data, where the synthetic-derived variations are plotted with the observed travel-time shifts at both stations. The match is quite good in character, magnitude and timing. The first unstable wavelet at VCA corresponds well to the PF_2PP reflection from the fault zone. At JCN the pattern of steady increase in the travel-time shift due to progressive involvement of slower S waves is quite clear.

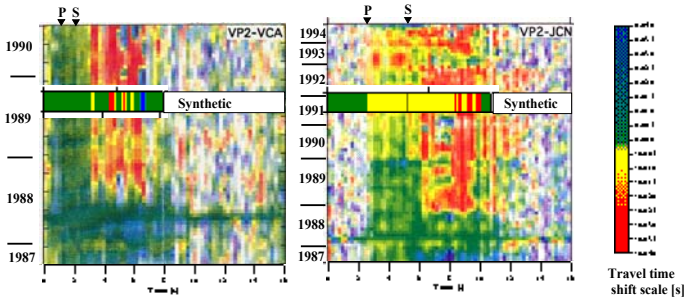

Figure 6. Comparizon of the observed and modeled variations [8].

While, previous studies clearly detected real changes in travel-times this modeling result supports that hypothesis and offers a more quantitative model for the actual wave propagation involved. The final link in the puzzle lies in the responsible mechanism for the velocity change in the fault zone. We are inclined to accept the idea of a deeper tectonic deformation that somehow changes the fluid environment in the shallow fault zone. The striking importance of the shallow vertical velocity gradient cannot be overstated. It is clear from this study that surface sources employed in highly heterogeneous environments such as the San Andreas fault zone can be expected to generate an overwhelming near-surface wave field that must be dealt with in looking for deeper images. If the individual phases can be identified, however, they may provide an important tool for studying near-surface details of the fault structure.

GUIDED WAVE IMAGING OF SAF CORE

A growing body of observations and numerical models testify to the imaging power of FZGW to characterize, spatially and temporally, properties and processes within the central cores of major active fault zones. Fault-zone guided waves were identified as such by Aki and co-workers in active-source surface-to-borehole studies and later in seismograms recorded in or near the fault zone from local earthquakes [11,12]. These waves are most visible for sources within a well-developed fault zone and receivers located within the same fault zone segment [13,14] although they appear also to be generated by off-fault surface sources [8]. The FZGW appear to be trapped by the presence of material in the fault that has a lower seismic wave velocity than the surrounding, more intact rock, from which it is separated by relatively sharp boundaries. The low-velocity nature of the San Andreas Fault zone core has long been recognized [15]. FZGW are seen in the codas of both the direct P and S waves, but they are usually much stronger in the S-wave coda, with large amplitudes in some cases arriving as late as twice the S-wave travel time [4]. They usually exhibit lower frequency content than the direct P or S waves and in many cases they appear to be dispersive.

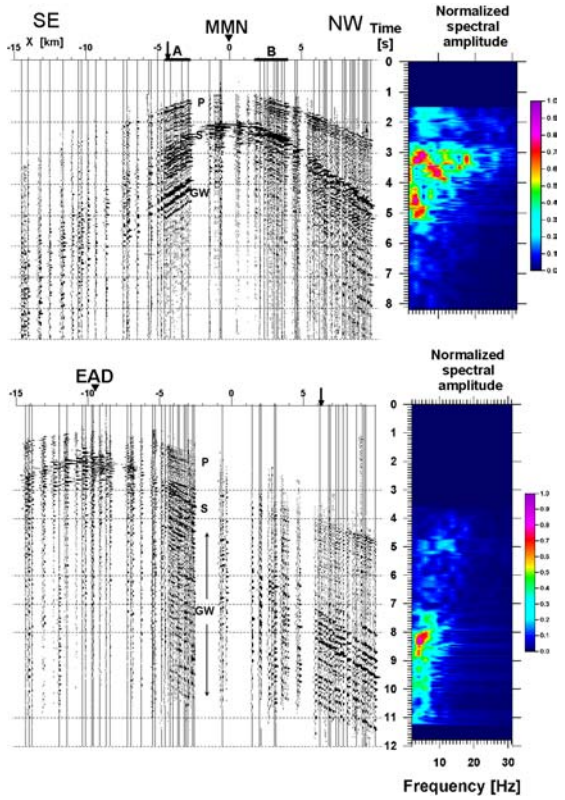

Figure 7. Left panels. Record sections or station gathers of horizontal-component seismograms for stations MMN and EAD, that constitute a reversed profile of sources (all with the same strike-slip mechanisms) in the depth range 3.3 to 3.8 km along a 35 km stretch of the fault zone (the 1966 M6 epicenter is at 0 km). 102 traces are shown for MMN, 84 for EAD, having been stacked in 10-m bins from 531 and 351 initial traces. FZGW are clearly evident in the coda of the S wave, and they are also seen in the P-wave coda. Note the systematic spatial variability in the FZGW, with strong generation for sources SE from MMN, but NW from EAD - i.e., the same earthquakes do not produce FZGW at both stations.

Right panels. Amplitude spectra for selected traces (arrows on sections) computed for moving window of 500 ms along the seismograms. Offset distances are -4.5 km for MMN and 8km for EAD. Note the very low frequency (3-8 Hz) content of the FZGW that is not seen in the direct P- and S- wave arrivals, even though the FZGW energy has been derived from those phases [3].

There are compelling reasons to study the FZGW phenomenon. First is the potential for defining the structure of the active fault zone at depth. Second, the features that bound rupture extent in large earthquakes (segmentation boundaries, gaps, streaks, or asperities) may be evident in FZGW generation and propagation characteristics. Finally, the degree to which processes underway in the cores of seismogenic fault zones can be detected and monitored is unknown, but of critical importance in seismology. Detection of transient or systematic changes within the fault core through successful FZGW imaging in four dimensions is a potentially powerful monitoring method [16].This is particularly true at Parkfield where the San Andreas is a low-velocity zone striking near-vertical [17] that clearly acts as a waveguide for seismic energy from earthquakes and surface sources [14,8]. Velocity models also show a high Vp/Vs ratio along the fault near the surface and at depth within the fault zone, and a pronounced vertical velocity gradient in the upper 2 km of the section. The geometry of the Vibroseis source and receiver network, the approximate two-dimensionality of the fault zone in the region of the traveltime anomaly, and the existence of detailed P- and S-wave velocity models for the area all combine to provide well-determined constraints in modeling FZGW observations. Numerical modeling and microearthquake data

indicate that FZGWs propagate within a San Andreas fault zone that is 100 to 200 m wide at seismogenic depths and with 20%-40% lower shear-wave velocity than the adjacent unfaulted media. The initial step in our FZGW investigation on the SAF was to look at the nature of FZGWs with respect to the hypocenter source location and receiver position, in order to map any obvious features in the spatial relationship of source and receiver. Two stations are close enough to the fault zone to provide a conveniently "reversed" profile of sources along the fault by building "station gathers" of traces.

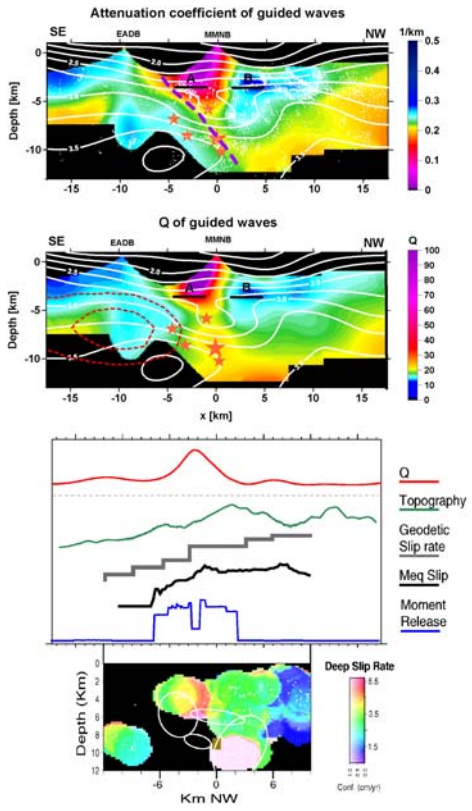

Figure 8. Spatial relationship of the FZGW attenuation/Q anomaly with other observations along the Parkfield segment of the San Andreas fault zone. Top 2 panels show in-fault attenuation and Q images resulting from the FZGW tomographic reconstructions. Note the zone of low FZGW attenuation (high Q) in the central portion of the panels delineating the transition at depth of locked to creeping fault (purple dashed line is our interpretation of the locked-creeping boundary at depth). Also shown are Vs contours, 1987-1998 seismicity (white dots and small red stars for the 4 recent M>4 events), and the 1966 M6 hypocenter (large red star). Interseismic slip rate distribution from [18] is shown in thick dashed red contour lines on the top of Q image. The third panel shows the function of FZGW Q taken along a profile at 3.5 km depth. Shown immediately below the Q curve are curves representing topography along the fault (green), surface fault slip rates from geodetic data (from [18] in grey), slip rates in the depth range 0 to 5 km inferred from recurrence intervals of characteristic microearthquake sequences (black), and the 1987-1998 moment release along the fault from SE to NW (blue). The bottom panel shows the along-fault deep-slip rate distribution at Parkfield inferred from the recurrence times of characteristic microearthquakes occurring between mid-1992 and 1995 (inclusive, see Nadeau and McEvilly, 1999), and the aftershock regions of the M>4 earthquakes occurring during this time period. Along fault features in all these characteristics correlate spatially and appear to delineate the same transition from locked to creeping behavior on the surface and at depth on the SAF at Parkfield [3].

Waveform coherence is strong along the profile because a common strike-slip mechanism dominates the mode of slip on the fault. This allows stacking of waveforms from nearby sources for enhanced signal-to-noise (Figure 7). The frequency content of typical waveforms that contain strong FZGWs is also shown in the figure. Note the low-frequency content not seen in the direct P and S waves that characterizes the FZGW arrival. Our results confirm that FZGW at Parkfield are generated within the fault zone and that they are most prominent late in the coda of S, while also seen in the P coda.

The attenuation of guided waves inversion result is shown in Figure 8 together with other geophysical data. The actual physical mechanism for Q variation within a FZ remains unknown. Most likely it is associated with fracture closure and opening caused by the evolution of stress induced changes in loading. Laboratory measurements of time lapse seismic attenuation of fractured rocks under increasing normal load show an initial steady increase in Q (due to closure of preexisting micro-fractures in the rock) that reaches a maximum value plateau and then decreases rapidly (due to the formation of new fractures) just prior to catastrophic failure of the rock [19].

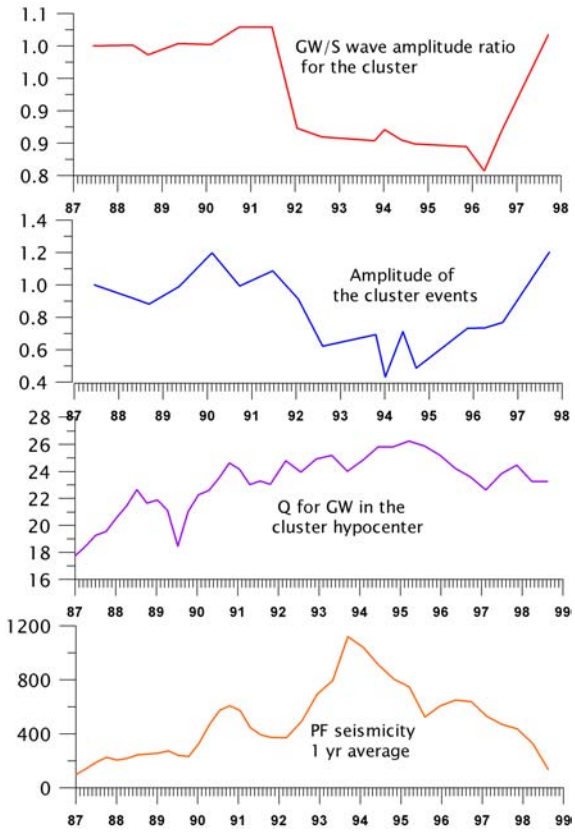

Figure 9. Observed changes during years 1987-1999 in Parkfield, California (upper three panels) compared with average seismicity (lower panel). Shown are attenuation factor Q for the cluster hypocenter (pink), amplitude of the cluster events (blue), and Guided wave/S wave amplitude ratio (red). Guided wave amplitude changes are the most profound while there was no detectable changes found in traveltimes.

The spatial distribution of Q at Parkfield indicates that a similar process may be occurring within the zone of concentrated stress build-up and release associated with the magnitude 4 and 5 earthquakes. The process of fracture closure and opening is also expected to involve dewatering and saturation of rocks (respectively) and corresponding changes in water pressure, all of which are expected to result in variations seismic propagation. We interpret the localized zone of FZGW low attenuation to be the NW edge of the M6 asperity at Parkfield at the transition of locked and creeping behavior of the SAF at depth with the high Q due most

likely to dewatering resulting from fracture closure and/or fault-normal compression. A greater understanding of the relationships between FZGW attenuation, and stress related fracturing processes under conditions of accumulating fault stress will be needed to obtain information useful for understanding the earthquake nucleation process and for possibly predicting earthquakes. A particular strength of using FZGWs to study the detailed structure and deformation of an active fault zone is that FZGW propagation is confined to the fault core.

This makes them highly sensitive to any spatial or temporal variations along the fault. In contrast, the propagation paths of direct P- and S- waves from earthquakes occurring within the low-velocity fault zone take place largely outside of the fault core in the higher-velocity country rock. As a result, direct P- and S- arrivals contain little information on the properties of the fault itself. This limits the resolution on fault structure that direct P- and S- can provide to about 5 km. In contrast, we have already shown that FZGWs can resolve the details of fault structure on the order 50m (Korneev et al. 2000). By increasing the number of receiver stations located directly on the fault, it should be possible to improve resolution even further. Preliminary analysis of seismograms from a cluster of 12 microearthquakes exhibit practically identical waveforms, although the magnitudes of the events belonging to that cluster clearly show strong temporal variations. The ray paths of this cluster intersect the FZ attenuation anomaly,which was found by tomographic inversion. Cross-correlation of the waveforms of the cluster reveal no traveltime changes for all recorded phases, including direct P, S, and guided waves. In contrast, amplitudes of guided waves show strong changes compared to P- and S-wave amplitudes. These changes correlate spatially and temporally with overall Parkfield seismicity, suggesting their common origin (Figure 9).

FAULT CONTINUITY TESTING

Low velocity layers continuity is a very important problem in geophysics. There are promising results from exploration geophysics demonstrating an ability of guided waves to propagate in low velocity sedimentary layers at distances substantially exceeding those of regular body waves [20,21]. We performed a numerical experiment to study guided waves propagation along curved waveguide. Such structures model ancient riverbed meanders, which contain low velocity sediments. An S shaped low velocity layer model was built having rather low 10% contrast. The velocity in outer media was 11 000 ft/s when velocity in the layer was 10 000 ft/s. Seismic waves were generated by horizontal dipole source. On the Figure 10 the propagating is shown in 4 snapshots, guided waves are clearly contained within the layer.

There is very interesting effect revealed by this experiment when propagating guided waves skid during propagation along curvatures and radiate body waves into bounding media. This experiment suggests existence and potential utilization of guided waves energy for seismic interpretation. For seismology, knowledge about a fault structure and composition has a critical significance for understanding of modeling and prediction of future earthquake scenarios. Seismic hazard in California is and will remain high mainly because of the San Andreas Fault events as a result of relative movement of two continental plates with average speed of about two centimeters per year.

Figure 10. Modeling of guided waves propagation along the

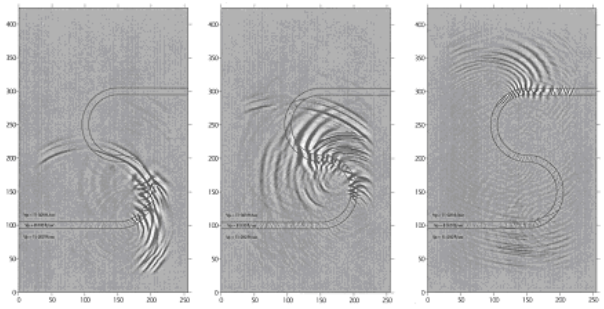

10% contrast curved wavegude [20].

This fault was a source of numerous strong earthquakes including catastrophic 1857 event with ruptures along a giant distance from Central California down to Los Angeles area, 1906 San Francisco event, destroying the city and most recent Loma Prieta 1989 earthquake. The last magnitude 6 event in Parkfield occurred in 1966, where it repeats in average every 20 years. The significance of the Parkfield area is in it being a transition zone between creeping NW and locked SE sections of SAF, which makes it a most likely spot defining future seismic activity of the region. The detailed studies of seismicity generated by Parkfield 1996 M6 event revealed very high seismic activity in Cholame valley region SE of the Parkfield and ruptures along Cholame valley tracing the fault along the surface. In the middle of the valley SAF has about 1.5 km jog to SW after which it continues to go in SE staying parallel to the original direction. The jog geometry had no surface evidence and was determined on the basis of epicenter locations of multiple events in this area. Seismic and theoretical studies

Figure 11. Steep-angle light imaging reveals details of small-scale topography in Cholame valley, which suggests an existence of echelon of faults berween SAF strands. Red line indicates the current mapping of the SAF trace.

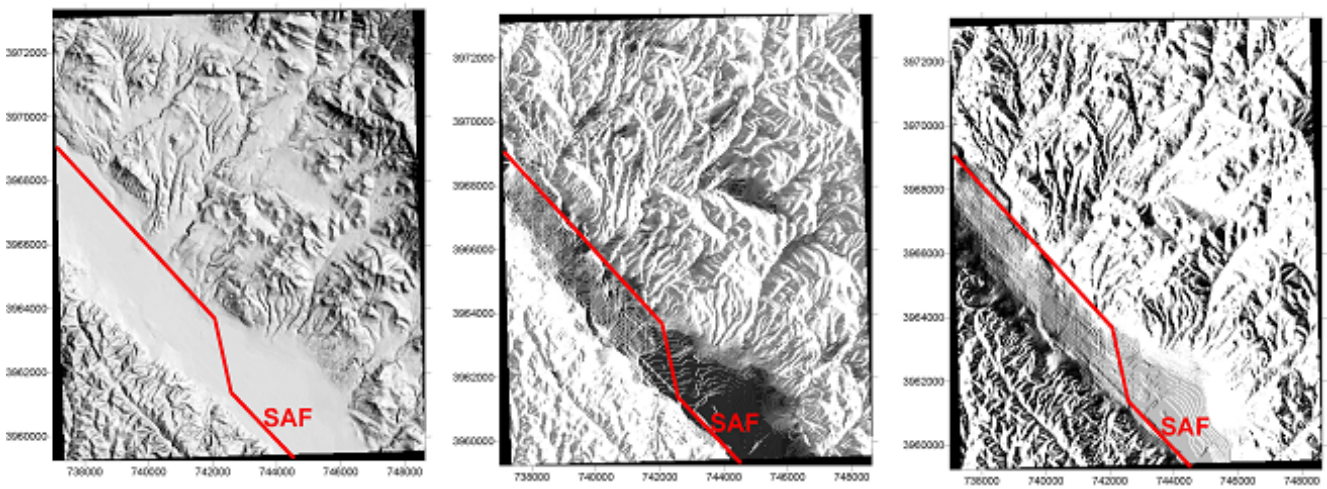

[22,23,18] suggested complex structure of the jog area, being and interacting segment of two parts of SAF. Such segments usually represent wide zones with multiple fractures oriented at 45 degrees with respect to main fault orientation and which connect isolated segments of a fault. The corresponding micro fracturing was

observed in multiple locations of Cholame valley. Extent and mechanical properties of interacting segments have strong impact on accumulated strain release. The fault structure studies in Cholame valley are mostly based on seismic information since valley sediments cover bedrock and do not allow accurate fault mapping. Nevertheless we have found that low amplitude topography features of the valley apparently affected by bedrock surface geometry. We used shade relief images analysis varying color saturation and light source position. The shade relief technique has spatial differentiating properties and allows simultaneous (Figure 11) of delicate, as well as pronounced topography details. An existing proposed point of jog connection with South-West strand of SAF. The fault can be traced along both sides through this point. Multiple NS oriented faults which make 45-degree angles with traces of SAF are quite visible. Image features also suggest a straight continuation of NW part of the SAF in SE direction after passing the jog. In the same time the NW straight extension of SE part of the SAF connects it with and mapped parts of South-West Fracture Zone (SWFZ), which extends quasi-parallel to SAF.

This result suggests the Cholame valley fault structure represent two faults which were separate at some point in history but began interacting through development of zone of shear faulting in the middle of the valley leaving some of their old parts temporarily inactive. This hypothesis can be tested using fault zone guided waves since inactive faults still should have low velocity properties due to relatively high concentration of fractures within the zones. The correspondent experiment will include excitation of fault zone guided waves by placing explosion and/or vibro seismic sources on a known existing fault zone (in particular on SWFZ) with surface seismic line recording across the anticipated trace of this fault at 5-10 km distance from the source. Detection of FZGW will indicate continuity of low velocity property along the source receiver path to support the suggested model for a fault structure.

CONCLUSIONS

Monitoring changes associated with processes in the core of the fault zone should provide valuable information about the fault condition and potentially lead to a better understanding of strong earthquakes. Use of a controlled source for guided wave monitoring is most desirable since the exact source location and initiation time are known. Explosion sources are not highly repeatable and require special permissions and precautions. A conventional Vibroseis source cannot be used for this study since its lowest excitation frequency is around 8 Hz, while FZGWs energy is in the 3-6 Hz band. Recent microearthquake analysis from the most active Hayward fault section (in Northern California) revealed presence of strong guided waves having even lower frequencies in the 2-5 Hz frequency range. Lowfrequency vibrators would be an ideal source for fault zone monitoring using guided waves. With modern modeling techniques FZGWs can provide detailed images of a fault zone's inner structure and other characteristics that may eventually lead to a better understanding of the nucleation process of large earthquakes and to their short-term prediction, but the relations between FZGW parameters, fault zone rock deformation, and fluid involvement need further investigation.

Parkfield is an ideal location a number of important experiments due to its high earthquake hazard, relatively regular recurrence interval, and long-term monitoring of various geophysical observables. Understanding the detailed structure, physical properties and evolution of the fault at depth is critical to advancing our knowledge of earthquake physics and for formulating estimates of earthquake hazard and developing schemes for hazard reduction. FZGW studies show promise for identifying blind faults and fault continuity across jogs and at depth.

ACKNOWLEDGMENTS

Data processing was done at the Center for Computational Seismology (CCS) at LBNL, which is operated by the University of California for the U.S. Department of Energy (DOE) under contract No. DE-AC03-76SF00098. The USGS provided financial support for this research through NEHRP award 1434-95-G-2540.

REFERENCES

[1]Bakun, W.H. and A.G. Lindh, The Parkfield, California, prediction experiment, Earthq. Predict. Res., 3,285-304, 1985.

[2] Karageorgi, E., R. Clymer and T.V. McEvilly, Seismological studies at Parkfield: II. Search for temporalvariations in wave propagation using Vibroseis, Bull. Seismol. Soc. Am., 82, 1388-1415, 1992.

[3] Korneev, V. A., Nadeau, , R. M. and T. V. McEvilly , 2003, Seismological Studies at Parkfield IX: Fault Zone Imaging using Guided Wave Attenuation , Bull. Seism. Soc. Am., vol.93,#4, 1415-1426.

[4] Karageorgi, E.D., T.V. McEvilly, and R.W. Clymer, Seismological studies at Parkfield IV: Variations incontrolled-source waveform parameters and their correlation with seismic activity 1987-1994, Bull.Seism. Soc. Am., 1996.

[5] Roeloffs, E., Persistent water level changes in a well near Parkfield, California, due to local and distantearthquakes, J. Geophys. Res., 103 (B1), 869-889, 1998.

[6] Langbein, J., R. Gwyther, R. Hart, and M.T. Gladwin, Slip rate increase at Parkfield in 1993 detected by high-precision EDM and borehole tensor strain meters, Geophys. Res. Lett., 26, 2529-2532, 1999.

[7] Nadeau, R.M., and T.V. McEvilly, Fault Slip Rates at Depth from Recurrence Intervals of Repeating Microearthquakes, Science, 285, 718-721, 1999.

[8]Korneev, V.A., T.V. McEvilly, and E.D. Karageorgi, Seismological studies at Parkfield VIII: Modeling theobserved travel-time changes, Bull. Seismol. Soc. Am., 90 (3), 702-708, 2000.

[9] Daley, T.M., McEvilly, T.V., Update of Shear-wave anisotropy measurements at the Parkfield Varian well, Seism. Soc. of Am., Annual Meeting, 1991.

[10] Daley, T.M., and T. V. McEvilly, Shear-Wave Anisotropy in the Parkfield Varian Well, Bull. of the Seism.Soc. of Am., 80, 857-869, 1990.

[11] Leary, P.C., Y.-G. Li, and K. Aki, Borehole observations of fault zone trapped waves, Oroville, CA, Trans.EOS Trans., 66, 976, 1985.

[12] Li, Y.-G., P. C. Leary, K. Aki and P. E. Malin, Seismic trapped modes in the Oroville and San Andreas fault zones, Science, 249, 763-766, 1990.

[13] Li, Y.-G., J.E. Vidale, K. Aki, C. Marone, and W.H.K. Lee, Fine structure of the Landers fault zone;segmentation and the rupture process, Science, 265, 367-370, 1994.

[14] Li, Y.-G., W. L. Ellsworth, C. H. Thurber, P. E. Malin and K. Aki, Fault-zone guided waves from explosions in the San Andreas fault at Parkfield and Cienega valley, California, Bull. Seism. Soc. Am.,87, 210-221, 1997.

[15] Feng, R. and T. V. McEvilly, Interpretation of seismic reflection profiling data for the structure of the San Andreas fault zone, Bull. Seism. Soc. Am., 73, 1701-1720, 1983.

[16] Li, Y.-G., J.E. Vidale, K. Aki, F. Xu and T. Burdette Evidence of shallow fault zone strengthening after the 1992 M7.5 Landers, CA, earthquake, Science, 279, 217-219, 1998.

[17] Michelini, A. and T.V. McEvilly, Seismological studies at Parkfield: I. Simultaneous inversion for velocity structure and hypocenters using B-splines parameterization, Bull. Seism. Soc. Am., 81, 524-552, 1991.

[18] Harris, R. A. and P. Segall, Detection of a locked zone at depth on the Parkfield, California, segment of theSan Andreas Fault, J. Geoph. Res., 92, 7945-7962, 1987.

[19] Sobolev, G.A., Babichev, O.V., Los,V.F., Kol'tsov,A.V.,

Ponomaryov,A.V., Ponyatovskaya, V.I., Rozanov, A.S., Stanchits, S.A., Khromov, A.A., Frolov, D.I., Yangquan,L., Jialiu,Z., Jiadong, Q. and L. Shiyu, 1996, Precursors of the destruction of water containing blocks of rock., J. Earthquake Prediction Research, 5.
[20] Korneev, V.A. and L.R. Myer, Testing of sedimentary layer continuity using guided waves, GRI topical report, 2001.
[21] Parra, J.O., Hackert, C., Gorogy, A and V.A. Korneev , 2001, Detection of guided waves between gas wells for reservoir characterization, Geophysics, Vol.67, No 1, p. 38-49, LBNL-48523.
[22] Hanna, W.F., S.H.Burch and T.W.Diblee, Gravity, magnetics, and geology of the San Andreas fault near Cholame, California: U.S. Geol. Surv. Prof. Paper 646-C, 1972.
[23] Eaton, J.P., M.E. O'Neill and J.N. Murdock, Aftershocks of 1966 Parkfield-Cholame, California Earthquake: A detailed study, Bull. Seismol. Soc. Am., 60 (4), 1151-1197, 1970.

Valeri Korneev,
90-1116, ESD, 1 Cyclotron Rd, Lawrence Berkeley National Laboratory, Berkeley, CA 94720, USA;: VAKorneev@lbl.gov

Robert Nadeau, Seismological Laboratory,
UC Berkeley, California, USA nadeau@seismo.berkeley.edu